We are IntechOpen, the world's leading publisher of Open Access books Built by scientists, for scientists

4,800
Open access books available

122,000
International authors and editors

135M
Downloads

Our authors are among the

154
Countries delivered to

TOP 1%
most cited scientists

12.2%
Contributors from top 500 universities

CLARIVATE ANALYTICS BOOK CITATION INDEX INDEXED

WEB OF SCIENCE™

Selection of our books indexed in the Book Citation Index in Web of Science™ Core Collection (BKCI)

Interested in publishing with us?
Contact book.department@intechopen.com

Numbers displayed above are based on latest data collected.
For more information visit www.intechopen.com

12

Condition Monitoring of Zinc Oxide Surge Arresters

Novizon[1,2], Zulkurnain Abdul-Malek[1], Nouruddeen Bashir[1] and Aulia[1,2]
[1]*Universiti Teknologi Malaysia (UTM),*
[2]*University of Andalas (UNAND),*
[1]*Malaysia*
[2]*Indonesia*

1. Introduction

Over voltages in power system may occur due to lightning, fault or switching operation. These overvoltages could reach dangerous amplitudes for power system apparatus. To protect the system electrical equipment and to guarantee an economic and reliable operation, surge arresters are applied in almost all types of electrical power network. Gapless zinc oxide (ZnO) surge arresters are widely used. The surge arresters are usually connected between the phase and ground terminals. They limit the voltage level in equipments such as transformers below the withstand voltage level.

Figure 1 shows the values of overvoltage which can be reached without the use of arrester in per units. The time axis is divided into the range of lightning overvoltage in microsecond, switching overvoltage in millisecond and temporary overvoltage in second. In the lightning overvoltage and switching overvoltage range, the magnitude of overvoltage can reach several per unit if the system is without arrester protection. Arrester could limit overvoltage below withstand voltage of equipment. This phenomenon clearly shows the importance of arresters for lightning overvoltage protection.

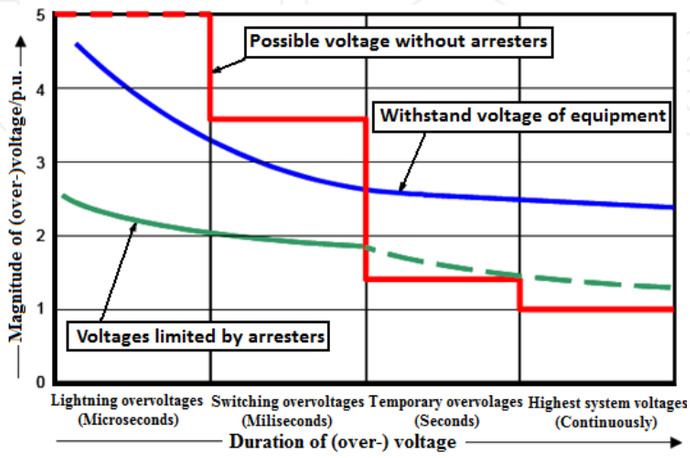

Fig. 1. Schematic representation of the magnitude of overvoltage

In this chapter, signal processing using LabVIEW is presented to separate the resistive leakage current from ZnO arrester leakage current using a novel technique called the Shifted Current Method for the purpose of monitoring the degradation of ZnO surge arrester.

1.1 Zinc oxide surge arrester

The construction of ZnO surge arresters consist of a very simple structure. They basically consist of an insulating housing which is made of porcelain or polymeric material, and the inner active column, composed of the ZnO varistors as shown in Figure 2.

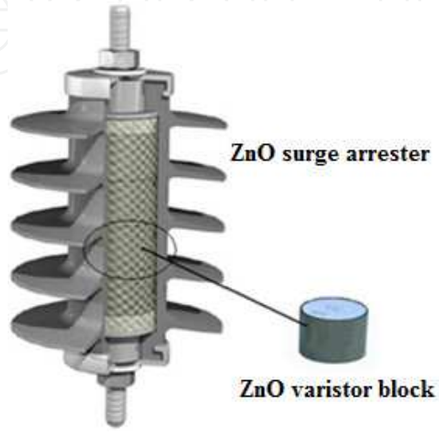

Fig. 2. The cross-section view of a polymeric insulated distribution class ZnO surge arrester

The ZnO varistor block elements are the main component of the ZnO surge arrester. They provide the desired non-linear characteristics and present a strong relation with the temperature (low current range). The non-linear resistivity is an inherent bulk property of the composite ceramic resistor, which consists of mainly ZnO with relatively small amount of several additives of other metal oxides such as Bi_2O_3, CoO_2, MnO3, and Sb_2O_3 (Eda, 1989). These additives essentially determine the electric properties of the block arresters element.

1.2 Voltage current characteristics of ZnO varistor block

The ZnO surge arrester element is composed of high-purity ZnO, which is the major constituent, and also slight amounts of some oxides of bismuth (Bi), cobalt (Co), manganese (Mn), antimony (Sb), and etcetera. These are thoroughly mixed, granulated, formed (pressed into a disc), specially treated to produce high-resistance layers on all sides of the element and finally sintered at a high temperature of more than 1000°C.

The blend ratio of ZnO surge arrester and additives is not constant but is about 9:1 (Kobayashi, 1986). The microstructure of this element is clarified by a secondary electron image taken by EMPA (Electron Probe Micro Analyzer). Figure 3 shows the secondary-electron image of the element. As shown in Figure 3, fine ZnO grains of 1 to 10 μm size can be seen.

The intergranular layer comprises mainly of Bi_2O_3 and spinel ($An_7Sb_2O_{12}$) distributed in the grain boundary. The excellent voltage-current nonlinear characteristics of the element may be attributable to the junction of the ZnO grain and the intergranular layer consisting mainly of Bi_2O_3. While the specific resistivity of ZnO grain is 1 to 10 Ωcm, that of the intergranular layer is as high as 10^{10} Ωcm and therefore almost all of the voltage applied to the element is concentrated on this high-resistivity intergranular layer. This layer possesses such a non ohmic characteristic that its resistance decreases suddenly at a certain voltage as the applied voltage rises.

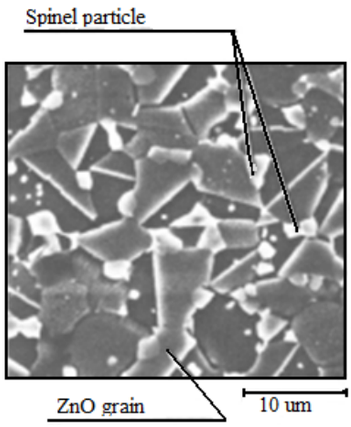

Fig. 3. Secondary-electron image of the ZnO element (Kobayashi, 1986).

The voltage-current characteristic of this layer shows an excellent non linearity throughout the range of 10^{-6} to 10^{4} A. The nonlinearity of this element is attributable to the combination of insulator (intergranular layer) and ZnO grain. Figure 4 shows the V-I characteristics of ZnO element which are divided into three regions, being low current region (I), operating region (II) and high current region (III).

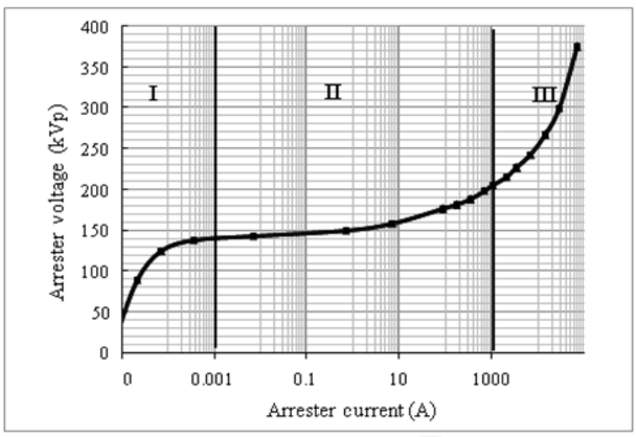

Fig. 4. Voltage-current characteristics of ZnO element (Eda, 1980)

The current density-electric field J-E, relationship in region I is expressed from the physical point of view as follows:

$$J = J_0 \exp\left\{-\frac{\phi - \beta E^{0}.5}{kT}\right\} \tag{1}$$

where $\beta = (e^{0.75}\,\pi\,\varepsilon\varepsilon_o)$, ϕ is the potential barrier (Â), E the electric field intensity (V/m), k the Boltzmann constant, T the absolute temperature (K), *e* the electron charge (C), ε_o the vacuum dielectric permittivity, and ε is the relative permittivity of the barrier substance.
Equation 1 clearly shows that, in low current region (I), the characteristics vary considerably with the temperature T. This region is located at a point where the line-frequency voltage is applied in applications for metal oxide arresters and it becomes important to pay attention particularly to the characteristic change with energized time and the temperature dependence.

In operating region (II), the current density is considered to be proportional to a power a of the electric field intensity and is explained by the Fowler-Nordheim tunnel effect:

$$J = J_0 \exp\left(\frac{\gamma}{E}\right) \tag{2}$$

where $\gamma = \frac{4(2m)^{\frac{1}{2}}}{3he}$, m is the electron mass, and h=ĥ/2π , with ĥ being the Planck's constant.
The nonlinearity is generally given by the following experimental expression:

$$I = CV^{\alpha} \tag{3}$$

where α = nonlinear exponent and C is a constant.
In applications of ZnO surge arrester this second region relates to protective characteristics when a lightning impulse current has flowed through the arrester. The greater the value of α, the better is the protective characteristics.
In high current region (III), the resistivity of ZnO grain is dominant and the characteristic is given by:

$$V \approx KI \tag{4}$$

where K is the resistivity of the ZnO grain.

1.3 ZnO arrester model

The non-linear voltage current characteristic of ZnO arrester in low current region (I) is generally represented by the equivalent circuit shown in Figure 5 (Lee, 2005). The resistor R_1 represents the non-linear resistance of the granular layers, where the resistivity ρ changes from 10^8 Ωm for low electric field stress to just below 0.01 Ωm for high stress. The equivalent capacitor C represents the capacitance between the granular layers with relative dielectric constant between 500 and 1200 depending on manufacturing process. R_z is the resistance of the ZnO grains with a resistivity of about 0.01 Ωm. To account for rate of rise effects, an inductor is included as shown in Figure 5. The inductance L is determined by the geometry of the current flow path.

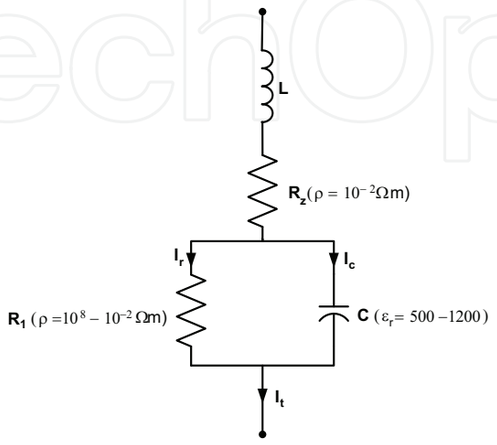

Fig. 5. Equivalent electric circuit of ZnO element

When R_1 and C changes, the capacitive current (I_c), and the resistive current (I_r) also change. The arrester's leakage current, in particular, the third harmonic component of the resistive leakage current, is known to be directly related to the degree of degradation of the ZnO arrester (Lundquist et al., 1990; Spellman et al., 1997; Zhou et al., 1998; Tang et al., 1999). In this work, in order to extract the resistive component from the total leakage current, the shifted current method (Abdul-Malek, et al. 2008) was used. The algorithm to extract the resistive component was implemented using the LabVIEW software.

The proposed method focuses on the ZnO arrester characteristic in low current region (I). In the low current region, R_z is much less than R_1 and the inductance L may be neglected. Therefore, in the continuous operating voltage region, the ZnO surge arrester is modelled as a non-linear resistor with a linear capacitive element in parallel as shown in Figure 6 (Haddad, et al. 1990).

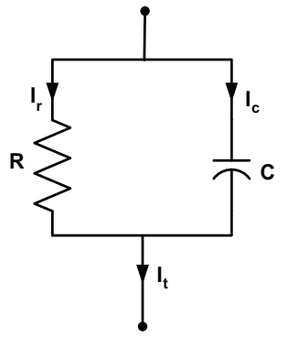

Fig. 6. Simplified equivalent model of a typical ZnO arrester

The total leakage current (I_t) of the arrester is given by a vector sum of a capacitive component (I_c) which does not vary with degradation of the arrester, and the resistive leakage current component (I_r) which varies with the degradation of the surge arrester. Figure 7 shows the typical phasor relationship of all these currents.

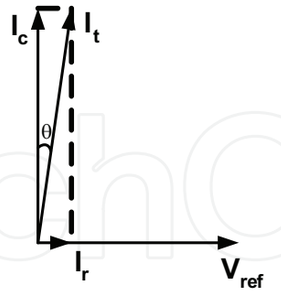

Fig. 7. Vector diagram of I_t, I_c, I_r and reference voltage.

All currents are time dependent, so I_t, I_c and I_r can be written as:

$$I_t(t) = I_r(t) + I_c(t) \tag{5}$$

The resistive current component can be obtained simply by subtracting the capacitive current component from the total leakage current as shown below:

$$I_r(t) = I_t(t) + I_c(t) \tag{6}$$

When system voltage is applied on the surge arrester at continuous operating voltage, about 80% of the rated voltage, the arrester experiences some leakage current. The amplitude of the leakage current depends on the condition of the surge arrester. The leakage current consists of the capacitive and the resistive current component. The typical specific capacitance of ZnO varistor block is 75 pF kV/cm^2. Typical values of the capacitive current range from 0.5 to 3 mA depending on the varistor diameter. For a complete surge arrester, the capacitive current depends on the number of varistor columns in parallel, the stray capacitances and actual operating voltage.

2. Shifted current method algorithm

One of the most common and straight forward techniques for extracting the resistive leakage current (LC) for the purpose of condition monitoring is the compensation technique (Shirakawa et al., 1998). In order to extract the resistive component from the total leakage current, the voltage across the arrester terminals is usually measured and used as a reference so that, based on the phase difference, the capacitive current component can be established. The resistive component is then obtained by just subtracting the capacitive component from the total leakage current. Other techniques to discriminate the resistive leakage current with the need of voltage as reference for the purpose of arrester condition monitoring have also been reported (Huijia et al., 2009; Kannus et al., 2007; Lira et al., 2007; Wenjun et al., 2008; Vitols et al., 2009).

Traditionally, measurement of total leakage current in substations or other installations was easily done using current shunts or current transformers, but the measurement of applied voltage to obtain the resistive LC make these techniques more appropriate in the laboratory rather than onsite due to the difficulty of measuring the voltage.

In this work, a new technique called the Shifted Current Method (SCM) is presented. This technique does not require knowledge of the applied voltage for the resistive leakage current to be obtained. The method is totally based on the manipulation of the total leakage current waveform. If the total leakage current is given by Equation 7 and the corresponding phase shifted (by a quarter of period) current by Equation 8, then the summation of these two waveforms can be written as Equation 9 below:

$$I_t(t) = I_t \cos(\omega t) \tag{7}$$

$$I_{tshifted}(t) = I_t \cos\left[\omega\left(t - \frac{1}{4f}\right)\right] \tag{8}$$

$$I_{sum}(t) = I_t\left[\cos(\omega t) + \cos\left\{\omega\left(t - \frac{1}{4f}\right)\right\}\right] \tag{9}$$

where $I_t(t)$ is the total leakage current, $I_{tshifted}$ is the shifted total leakage current (by a quarter of period of waveform), and I_{sum} is the summation of the total leakage current and the shifted current wave form. By signal manipulation technique, from this summation current, the capacitive component of total leakage current can be determined, and thereafter the resistive component of the leakage current can also be obtained by subtracting the capacitive component from the total leakage current.

Based on the above proposed technique, the algorithm to separate the resistive leakage current from the total leakage current was built. The algorithm for the shifted current method could be summarized as follows. Firstly, the arrester total leakage current is measured, and then a new waveform is introduced by shifting the measured arrester total LC by a quarter period of its operating frequency. Next, both the two total leakage currents are summed together and their peak time determined. The amplitude of summed total leakage currents at time T_p, where T_p is the time corresponding to the peak value of the summation waveform, is the peak value of the resistive current. The peak time obtained is used to determine the peak time of the capacitive current component which is equal to a quarter of period before or after the peak time of the resistive component. The peak value of the capacitive component is also determined from the original leakage current waveform. The capacitive leakage current is then generated based on the peak time, the peak value and the frequency detected. Finally, the resistive leakage current is obtained by subtracting the capacitive leakage current from the total leakage current. The block diagram of the algorithm for calculating the resistive leakage current using the shifted current method is shown in Figure 8.

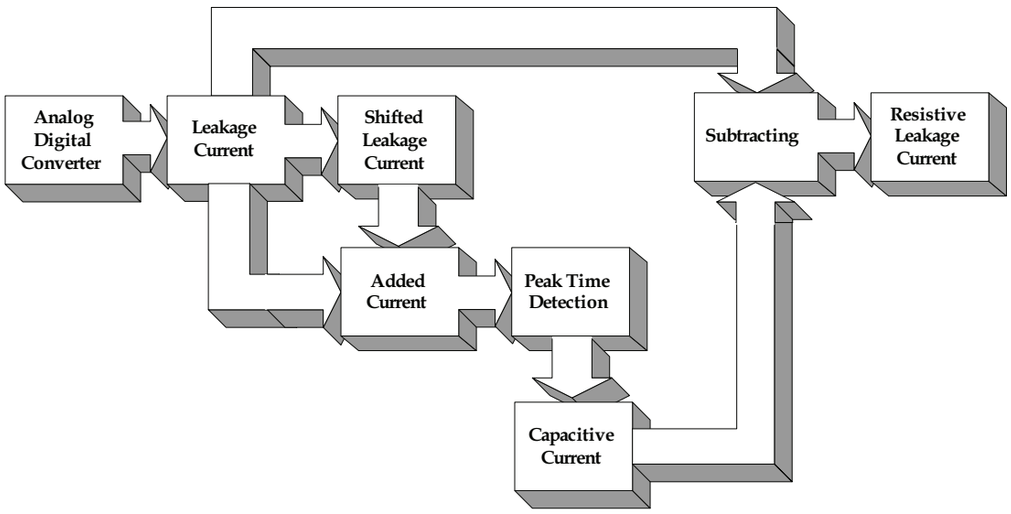

Fig. 8. Block diagram of the shifted current method algorithm

3. Implementation of method in LabVIEW

The shifted current method was implemented in NI LabVIEW 8.5 software. Each block was created and after that combined together to build an arrester monitoring system based on the SCM algorithm. The subsequent subsections explain the implementation of the SCM in LabVIEW.

3.1 LabVIEW-picoscope interface

Picoscope is a device that resembles the functions of an oscilloscope but runs on computer. Usually, Picoscope comes with software that turns it into a PC oscilloscope. In order to connect with LabVIEW, a VI (virtual instrument) interface was developed. LabVIEW Picoscope VI program links the Picoscope with LabVIEW software. The block diagram of the program is shown in Figure 9. The interface indicator shows a graph in front panel of the block diagram as shown in Figure 10.

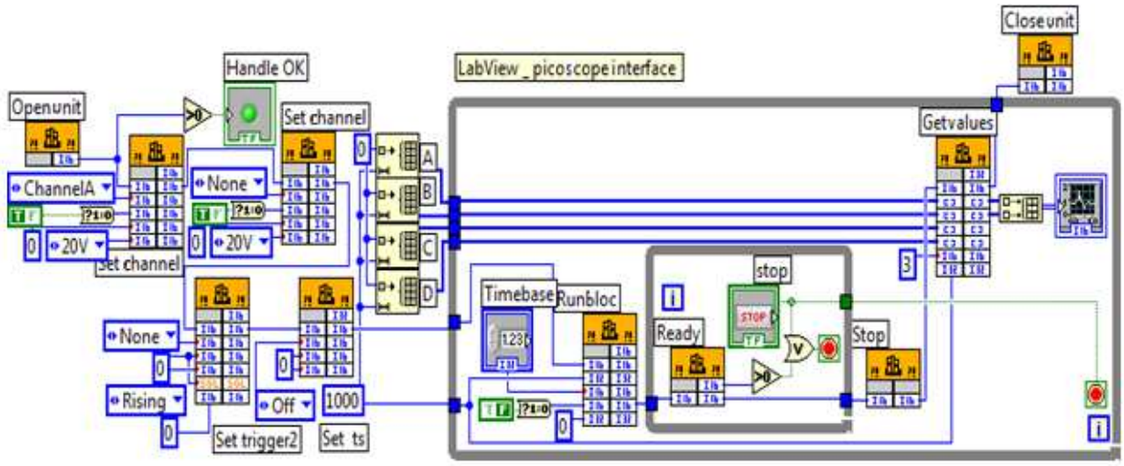

Fig. 9. NI LabVIEW-Picoscope VI interface block diagram

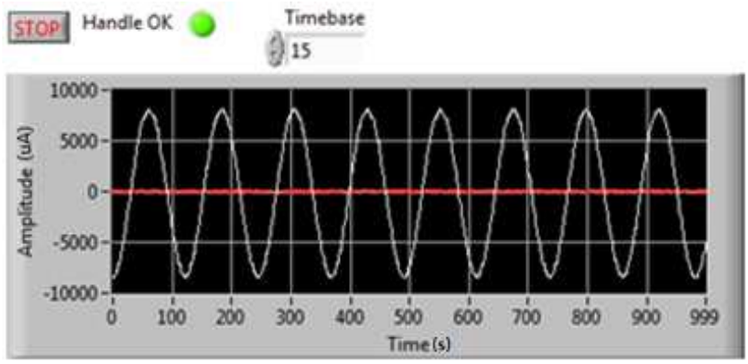

Fig. 10. Front panel of NI LabVIEW-Picoscope interface

3.2 Frequency detector block

The frequency detector block is a VI in the LabVIEW library as shown in Figure 11, used to detect the frequency, amplitude and phase of the surge arrestor total leakage current being measured. Figure 12 shows a typical output of the block in the form of front panel with the measured frequency, current and phase.

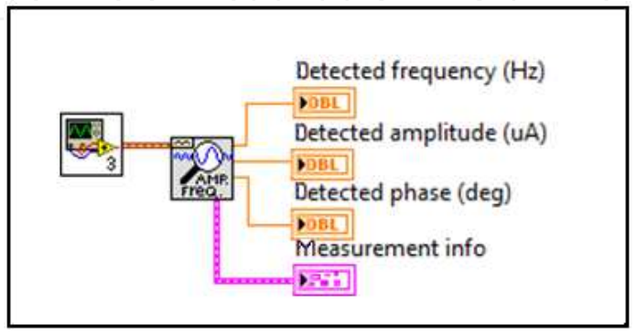

Fig. 11. Function of NI LabVIEW library for detecting frequency

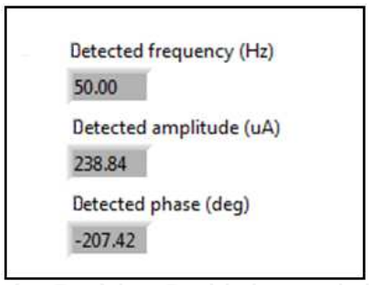

Fig. 12. NI LabVIEW front panel of frequency detector

3.3 Shifted signal block

This block was used to shift the total leakage current. In this block the total leakage current was generated and shifted to a quarter period of frequency. The frequency was detected using the frequency detector. It was then used as an input to the shifted signal block to shift the leakage current as shown in Figure 14. The time t to shift the total leakage current signal is given by

$$t = \frac{1}{4f} \tag{10}$$

where f is the signal frequency.

The frequency for this simulation is 50 Hz, so using Equation 10 the time to shift the current is 0.005 second. The signal was changed to array and shifted using NI LabVIEW Y[i-n].vi function as shown in Figure 13. The block diagram and front panel to shift the signal are shown in Figure 14 and Figure 15 respectively.

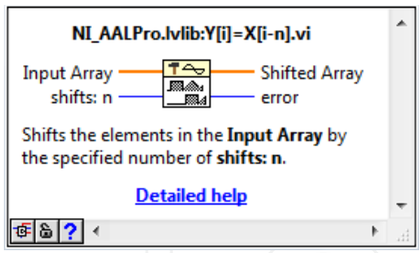

Fig. 13. Function of NI LabVIEW library for shifted array

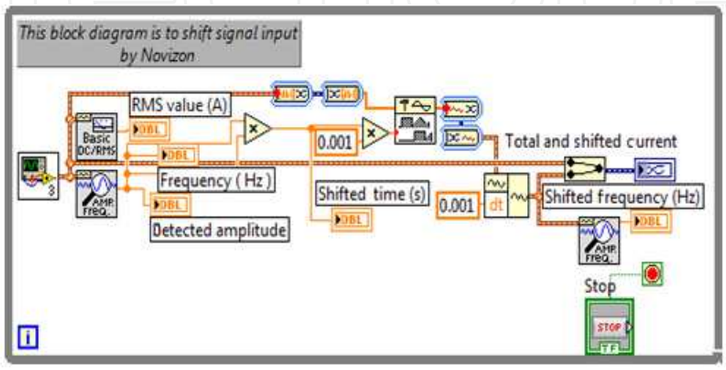

Fig. 14. The LabVIEW current shifting block diagram

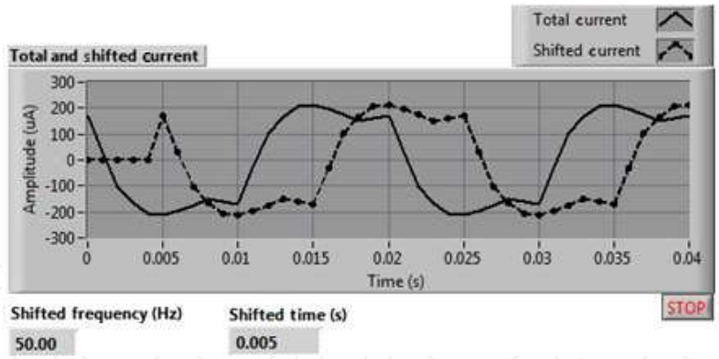

Fig. 15. Front panel of the current shifting

3.4 Adding signal block

The total leakage current and the shifted current were added using the adding block as shown in Figure 16. The result of the summation can be seen in Figure 17. The adding block is a simple block which was also available in LabVIEW library.

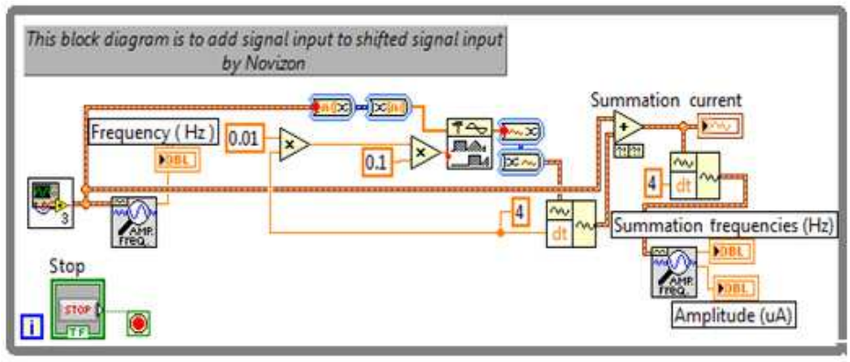

Fig. 16. LabVIEW block diagram of added signals

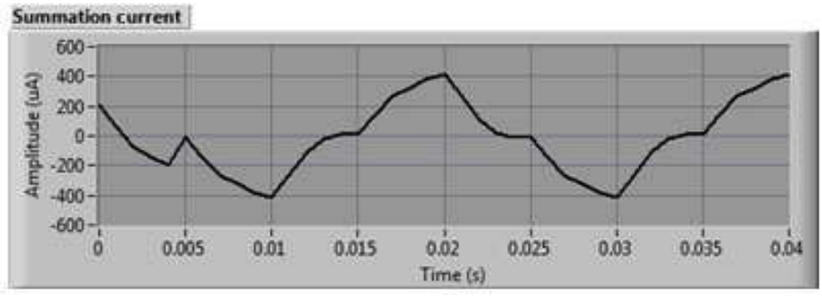

Fig. 17. Front panel of summed total LC signals

3.5 Peak time detector block

The peak of the summed total LC currents was detected using the peak detector shown in Figure 18. The time T_p was also detected. The block diagram of the peak signal detection consists of the peak amplitude and the corresponding time detection. Figure 19 shows the block diagram while Figure 20 shows the front panel indicating the peak and value of the parameter displayed on the front panel.

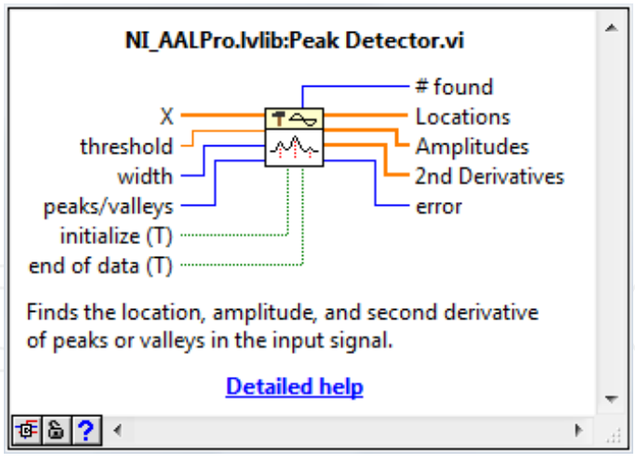

Fig. 18. Function of NI LabVIEW library for peak detector

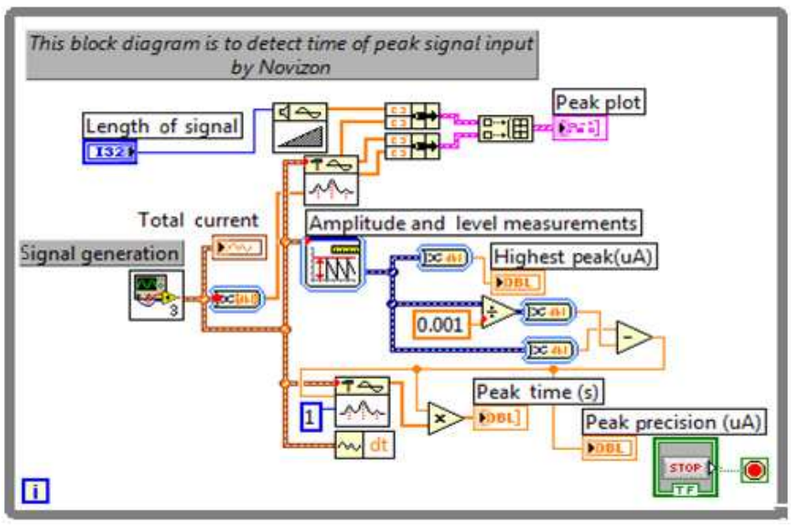

Fig. 19. LabVIEW diagram of peak detector

In the front panel, some easy-to-read parameters were also displayed. The parameters include the highest peak, the precision and the peak time. All parameters will be used in the xy determination block.

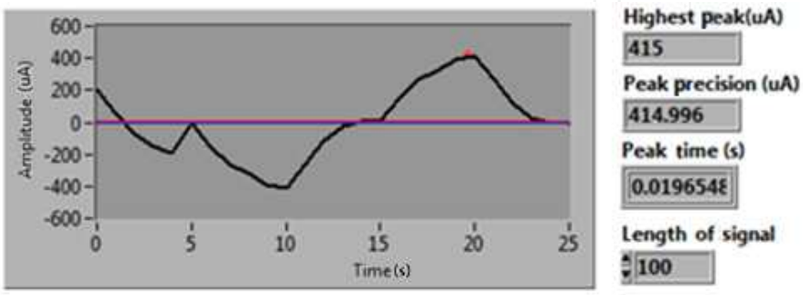

Fig. 20. Front panel of peak time detector

3.6 XY determination block

The peak value of the capacitive LC corresponds to the peak value of the summed total LC when a quarter of period of signal frequency is added to T_p. To do so, after the peak time T_p of the summed total LC was obtained, the value was then added with a quarter of period of the signal frequency. The XY determination block was then used to determine the peak value at that instant of time. Figure 21 shows the xy determination block.

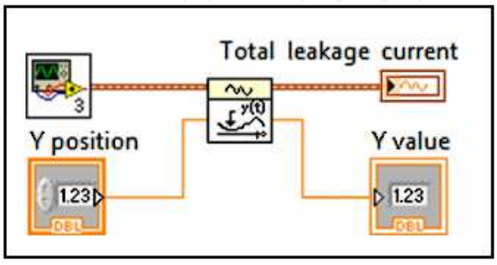

Fig. 21. LabVIEW diagram of XY determination

3.7 Signal generation block

After detecting the amplitude of the capacitive component of the total LC which corresponds to the y value of the XY determination block, together with the frequency of the total LC, a signal generator block shown in Figure 22 was used to generate the capacitive LC. The y value, the frequency and phase, were the inputs to this block and the output was a sinusoidal waveform as shown in Figure 23 and Figure 24.

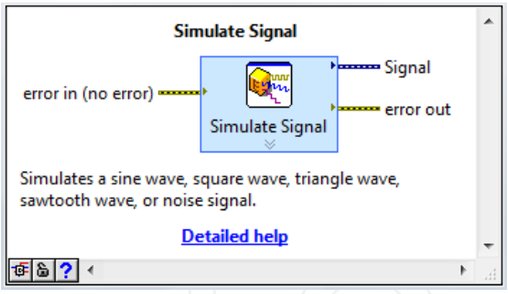

Fig. 22. Function of NI LabVIEW library for simulate signal

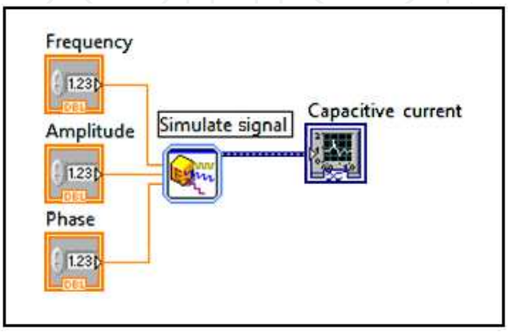

Fig. 23. LabVIEW diagram of capacitive signal generation

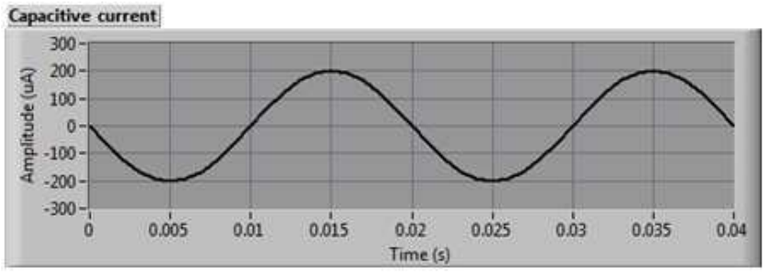

Fig. 24. Front panel of capacitive generation block

3.8 Resistive current extraction block

With the generation of the capacitive current obtained from the total LC, the resistive LC can be obtained by subtracting the total LC from the capacitive signal obtained using the signal generating block. This was achieved by simply using the LabVIEW subtracting block. Figure 25 shows the complete block diagram of this process. Figure 26 shows that capacitive and total leakage currents.

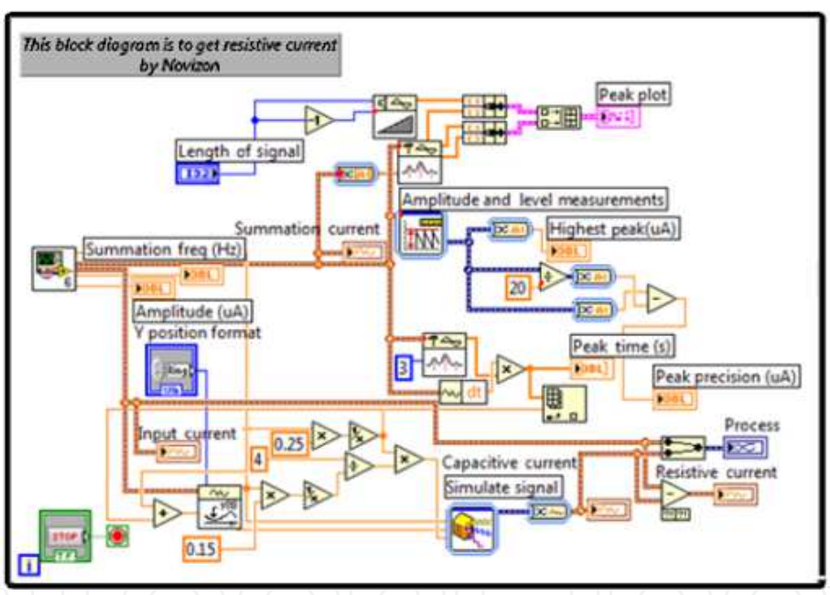

Fig. 25. LabVIEW block diagram of capacitive current discrimination

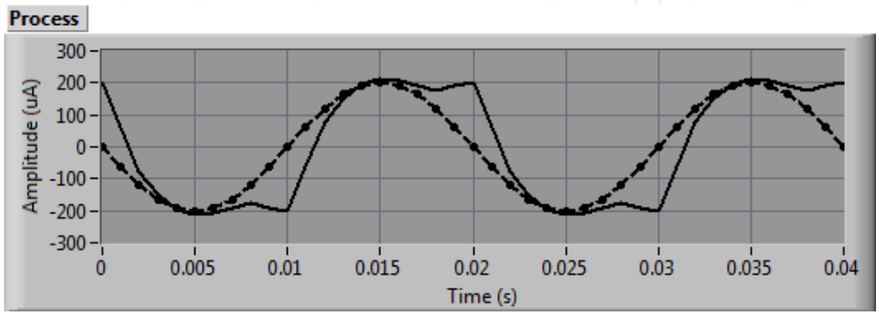

Fig. 26. Capacitive and total leakage currents

The result of this process which is the resistive component of the total leakage current can be seen in Figure 27. This resistive current contains harmonics because of the non linear characteristic of the ZnO material as well as the ageing effects. The third order harmonic of this resistive leakage current could be extracted using the Fast Fourier Transform (FFT).

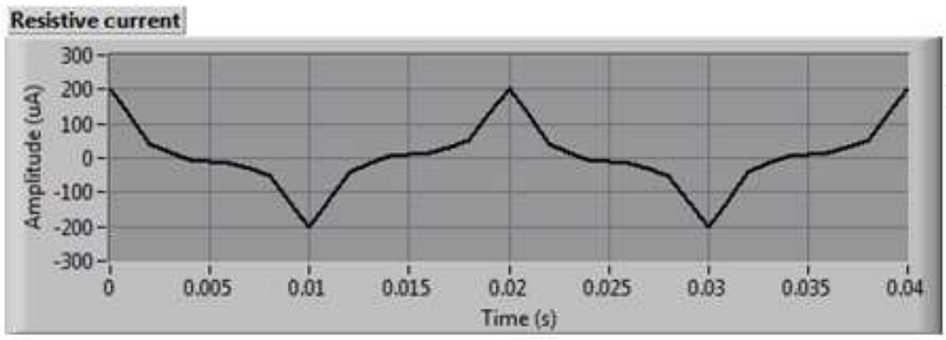

Fig. 27. The resistive leakage current

3.9 ZnO surge arrester monitoring system

All blocks which have been described above were combined to give a complete surge arrester monitoring system. The complete block diagram is shown in Figure 28.

4. Experimental results

Experimental work was conducted on a new zinc oxide (ZnO) arrester block in the laboratory. The ZnO arrestor block had a diameter and thickness of 40 mm and 21 mm respectively. Its rated voltage and discharge currents were 3 kV_{rms} and 10 kA. The arrester block's maximum continuous operating voltage (MCOV) was 2.55 kV_{rms}.

The total leakage current of the arrester block was measured using a 10 kΩ resistive shunt (power resistor) and the voltage using a capacitive divider with a ratio 686:1.

The total leakage current of surge arrester block or element that has not deteriorated will be dominated by capacitive LC thus having small resistive LC. When the zinc oxide element or block starts to experience degradation, the resistive LC gradually increases. In this study, for the zinc oxide block sample to experience increased resistive LC, voltages above the MCOV were applied (Shirakawa et al., 1998). The applied voltage was increased from 1 kV to 3.5 kV in steps of 0.5 kV. The results of measurement are presented in Table 1 and Figure 29 shows the graphical result for 3 kV displayed by the LabVIEW program.

Applied Voltage (kV)	I_T (mA)	Resistive Current (mA)	Leakage Current Harmonics			
			Fundamental	Third	Fifth	Seventh
1	0.150	0.065	0.053	0.021	0.005	0.003
2	0.165	0.075	0.061	0.032	0.006	0.005
2.5	0.288	0.137	0.094	0.059	0.032	0.018
3	0.53	0.458	0.512	0.117	0.063	0.041
3.5	0.707	0.512	0.558	0.239	0.076	0.054

Table 1. Measurement result using ZnO surge arrester monitoring system

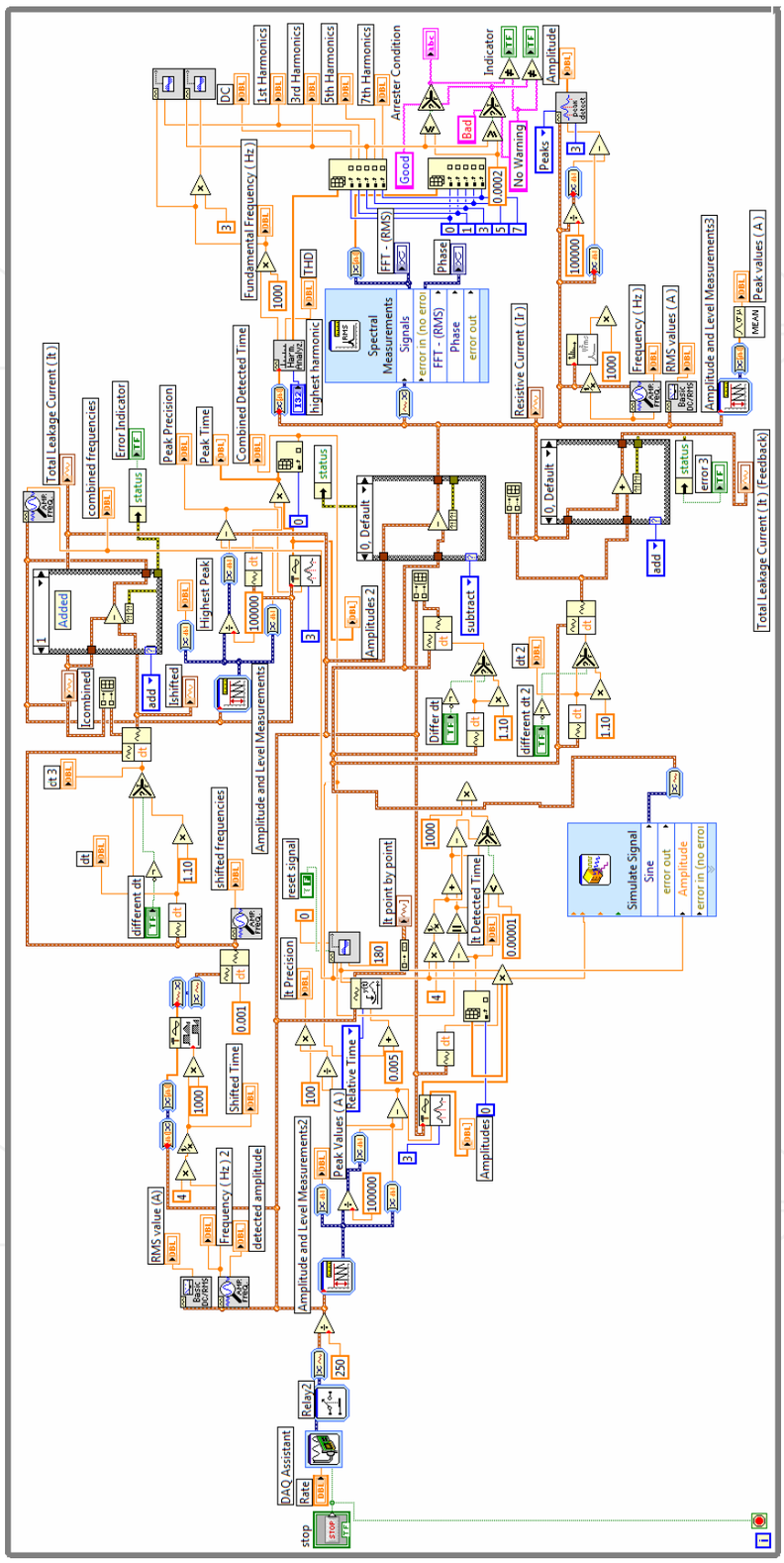

Fig. 28. LabVIEW block diagram of ZnO arrester monitoring system

It can be seen from Table 1 that the resistive current of the arrester block had low harmonics within nominal operating voltage (1 – 2.5 kV), suggesting it had not undergone degradation. As the voltage was increased beyond MCOV, the resistive LC as well as the LC harmonics especially the third harmonic increased exponentially indicating degradation.

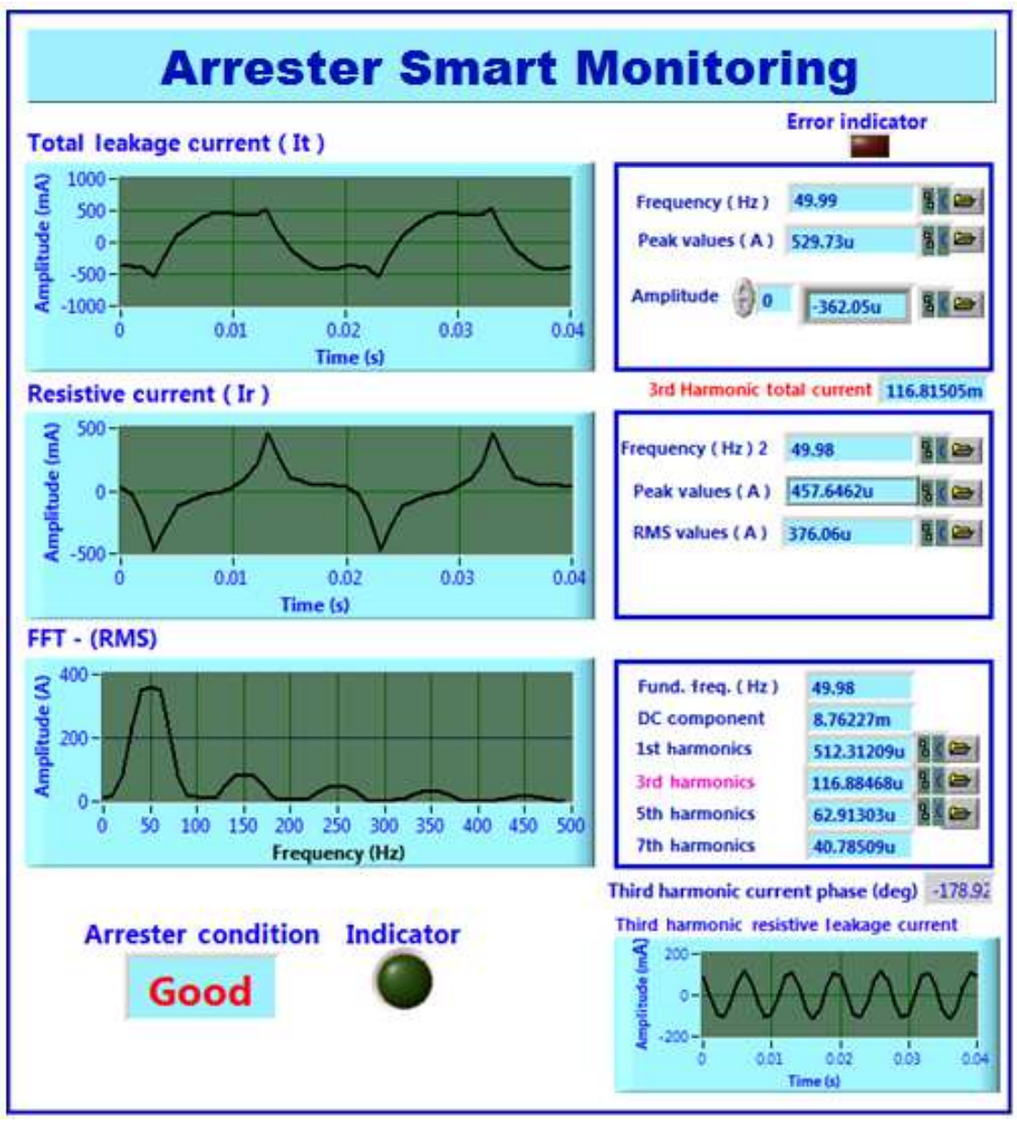

Fig. 29. Front panel of ZnO surge arrester monitoring system (applied voltage 3kV)

5. Conclusion

The new shifted current method technique to determine ZnO ageing was successfully implemented in LabVIEW software and proven useful for on-site measurement purposes. Field tests on the whole measuring and analysing system was successfully carried out. The developed program provides not only convenience in system management but also provides a user-friendly interface.

6. Acknowledgement

The authors would like to thank Ministry of Science, Technology and Innovation (MOSTI) Malaysia and Research Management Centre (RMC), Universiti Teknologi Malaysia, for the financial and management support.

7. References

Abdul-Malek Z. et al. (2008). A New Method to Extract The Resistive Component Of The Metal Oxide Surge Arrester Leakage Current, Proceedings of Power and Energy Conference (PECon), Johor Bahru, Malaysia, December 2008.

Abdul-Malek Z. et al. (2008). Portable Device to Extract Resistive Component of The Metal Oxide Surge Arrester Leakage Current, Proceedings of Australian Universities Power Engineering Conference (AUPEC), Australia, December 2008.

Eda, K. et al. (1980). Degradation Mechanism Of Nonohmic Zinc Oxide Ceramics, J. Appl. Phys., vol. 51, no. 5, pp. 2678–2684

Eda, K. et al. (1989). Zinc Oxide Varistors, IEEE Electrical Insulation Magazine; Vol. 5; No. 6; Nov-Dec 1989, pp. 28-41.

Haddad, A. et al (1991). Characterization of ZnO Surge Arrester Elements With Direct and Power Frequency Voltages, *IEE Science, Measurement and Technology*, vol. 137, No. 5, September 1991, pp. 265 – 272.

Huijia, L. et al. (2010). Development of Tester of the Resistive Leakage Current of Metal Oxide Arrester, Proceedings of Asia Pacific Power Engineering Conference, Chengdu, China, March 2010.

Kannus, K. et al. (2007). Laboratory Investigations of the Electrical Performance of Ice-covered Insulators and a Metal Oxide Surge Arrester, *IEEE Trans. Diel. Elect. Insul.*, Vol. 14, No. 6, December 2007, pp. 1357 - 1372.

Kobayashi, M. et al. (1986). Metal Oxide Surge Arrester, IEEE Transactions on Electrical Insulation Vol. EI-21 No.6, December, 1986, pp. 989 – 996.

Lee, B.H. and Sung, M.K, (2005). A New On-Line Leakage Current Monitoring System of ZnO Surge Arresters, *Journal of Material Science and Engineering B*, Vol.119,Issue 1, No. 15, May 2005, pp. 13 – 18.

Lira, J. G. A. et al. (2007). ZnO Surge Arresters Diagnosis Using Microcontroller, Proceedings of Instrumentation and Measurement Technology Conference Warsaw, Poland, May 2007.

Lundquist, J. et al. (1990). New Method For Measurement Of The Resistive Leakage Currents Of Metal-Oxide Surge Arresters In Service, IEEE Transactions on Power Delivery, Vol. 5, No. 4, November 1990, pp. 1811 – 1822.

Spellman, C.A. et al. (1997), A Technique for on-Line Monitoring of ZnO Surge Arrester, Proceedings of the 10th International Symposium on High Voltage Engineering, Canada, August 1997.

Tang, J. et al. (1999). Study of Multi-Coefficient Compensation Method on Resistive Current Passing Trough MOA, *High Voltage Engineering*, Vol.25, No.1, March 1999.

Vitols, A. P. et al. (2009). Condition Monitoring of Post Insulators and Surge Arresters, Proceedings of IEEE Electrical Insulation Conference, Montreal, Canada, May 2009.

Wenjun, Z. et al (2008). Design of on-line monitoring device for MOA used in 10kV distribution network, Proceedings of International Conference on Condition Monitoring and Diagnosis, Beijing, China, April 2008.

Zhou, L. et al. (1998). A Study on Variable Coefficient Compensation Method and Performance Diagnosis of Metal Oxide Arrester's Operating State Detection, Electric Technology Transaction, Vol. 13, No.6.

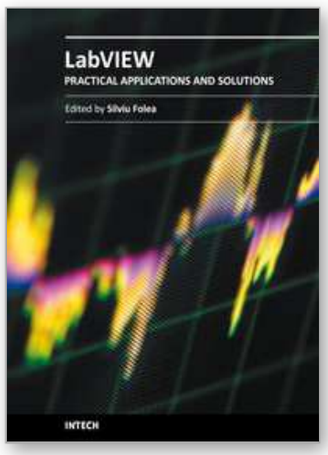

Practical Applications and Solutions Using LabVIEW™ Software

Edited by Dr. Silviu Folea

ISBN 978-953-307-650-8
Hard cover, 472 pages
Publisher InTech
Published online 01, August, 2011
Published in print edition August, 2011

The book consists of 21 chapters which present interesting applications implemented using the LabVIEW environment, belonging to several distinct fields such as engineering, fault diagnosis, medicine, remote access laboratory, internet communications, chemistry, physics, etc. The virtual instruments designed and implemented in LabVIEW provide the advantages of being more intuitive, of reducing the implementation time and of being portable. The audience for this book includes PhD students, researchers, engineers and professionals who are interested in finding out new tools developed using LabVIEW. Some chapters present interesting ideas and very detailed solutions which offer the immediate possibility of making fast innovations and of generating better products for the market. The effort made by all the scientists who contributed to editing this book was significant and as a result new and viable applications were presented.

INTECH
open science | open minds

InTech Europe
University Campus STeP Ri
Slavka Krautzeka 83/A
51000 Rijeka, Croatia
Phone: +385 (51) 770 447
Fax: +385 (51) 686 166
www.intechopen.com

InTech China
Unit 405, Office Block, Hotel Equatorial Shanghai
No.65, Yan An Road (West), Shanghai, 200040, China
中国上海市延安西路65号上海国际贵都大饭店办公楼405单元
Phone: +86-21-62489820
Fax: +86-21-62489821

IntechOpen